Topological origin of the fermion sign problem

Mauro Iazzi, Alexey A. Soluyanov, and Matthias Troyer
Theoretische Physik, ETH Zurich, 8093 Zurich, Switzerland
(Received 5 December 2014; revised manuscript received 18 May 2015; published 1 March 2016)

Monte Carlo simulations are a powerful tool for elucidating the properties of complex systems, but when applied to fermionic quantum systems, quantum Monte Carlo (QMC) algorithms suffer from the so-called "negative sign problem," causing the computational effort to grow exponentially with problem size. Here we demonstrate that the fermion sign problem originates in topological properties of the configurations. Using the widely used determinantal approaches, that remove the trivial sign problem due to particle exchange, we prove that the negative sign of a configuration is a topological invariant—an imaginary time counterpart of the Aharonov-Anandan phase—and reduces to a Berry phase in the adiabatic limit. This provides an intriguing connection between QMC simulations and classification of topological states.

DOI: 10.1103/PhysRevB.93.115102

The powerful method of Monte Carlo sampling can be applied to quantum systems by introducing an imaginary time formulation of the Schrödinger equation which describes classical particles performing a random walk in an external potential [1]. Identifying finite imaginary times with the inverse temperature $\beta = 1/k_B T$ has led to the path-integral formulation of quantum mechanics, where the partition function $Z = \mathrm{Tr}\exp(-\beta H)$ of the quantum system is mapped into a sum $Z = \sum_c w_c$ over the paths c with statistical weights w_c. The stochastic sampling of these paths forms the basis of finite temperature quantum Monte Carlo (QMC) algorithms, which have been widely applied to simulate quantum lattice models [2–5], the electronic structure of materials [6,7], ultracold atoms [8,9], nuclear matter [10], and lattice quantum chromodynamics [11].

While in classical systems the Boltzmann weights are always positive, in QMC the weight of a configuration can be negative due to particle statistics or gauge fields [12].[1] Negative weight configurations then cancel contributions of positive ones, resulting in an exponential increase of statistical errors with system size and inverse temperature (see Appendix A for details). The sign problem hence severely limits the applicability of QMC methods. While it is representation-dependent, which leaves hope for a solution, it is also nondeterministic polynomially (NP) hard [13]. This implies that unless $P = NP$ [14], which is believed to be highly unlikely, there is no generic solution.

Since the sign problem can be solved in specific cases [15–19], one may ask if a broader solution may exist for a restricted class of models, such as Hubbard models. The origin of the sign problem in these models has remained controversial and several, so far unsuccessful, attempts at a solution have been made [4,20–28]. In this paper we will show that the origin of the sign problem in common fermionic QMC approaches lies in topological properties of the path configurations and a nonzero Aharonov-Anandan phase picked up during evolution [29]. We will here only consider unbiased algorithms, ignoring approximations such as the *fixed node* approximation [30] which may modify the physics of the model.

The simplest QMC approach is the world-line algorithm (WL-QMC), which samples real-space world lines of particles evolving in imaginary time. Indistinguishable particles can be exchanged during the evolution, as sketched in Fig. 1. For fermions, an odd number of exchanges results in a final state that differs in sign from the initial state. After closing the trace it thus contributes with a negative weight. The topological nature of the sign problem, due to the braiding of fermions, is readily apparent. It implies that no local transformation can remove this sign problem but more drastic changes of the representation are needed. In some specific cases this sign problem might be removed by an ansatz on the distribution of positive and negative sign regions of phase space [31].

The hope to solve the sign problem by restricting the sampling to antisymmetric wave functions has prompted the development of determinantal QMC algorithms which have become state of the art in fermionic simulations [4,5,32–35]. Most of these are formulated in an *auxiliary field* approach which maps interacting fermions to noninteracting ones coupled to a fluctuating auxiliary field. Integrating out the fermions, one ends up with an action of only the bosonic auxiliary field. Nevertheless, contrary to initial expectations [36], these algorithms still suffer from an exponential sign problem whose origin has been controversially discussed [12,22,25,27,28,37–39].

To illustrate that the remaining sign problem is linked to a nontrivial value of a topological invariant, we will initially focus on the Hubbard mode, but note that our conclusions apply more generally. The Hamiltonian of the Hubbard model,

$$H = -t \sum_{\langle ij\rangle,\sigma} c^\dagger_{i\sigma} c_{j\sigma} - \sum_{i\sigma} \mu_\sigma c^\dagger_{i\sigma} c_{i\sigma} + U \sum_{i\sigma} c^\dagger_{i\uparrow} c_{i\uparrow} c^\dagger_{i\downarrow} c_{i\downarrow}, \tag{1}$$

describes fermions with spin $\sigma = \uparrow,\downarrow$, that hop between neighboring lattice sites with a matrix element t and interact via an on-site repulsion U. The spin-dependent chemical potential μ_σ combines the chemical potential μ and a Zeeman term. Our knowledge of the phase diagram of the Hubbard model remains incomplete, not the least due to the fermion sign problem.

To perform auxiliary-field QMC one discretizes the inverse temperature into small imaginary time steps $d\tau$. We use

[1] Similar sign problems can appear in other contexts when sampling sums and integrals that include negative terms, however we are here exclusively concerned with the sign problem arising from the use of quantum Monte Carlo algorithms to simulate a system of fermions.

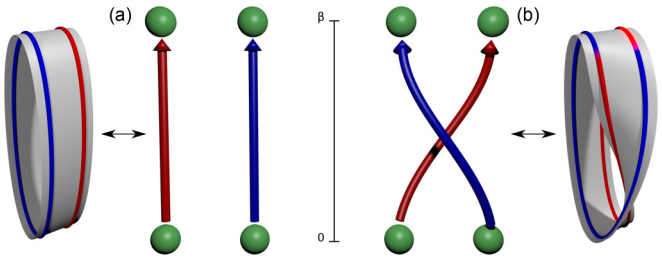

FIG. 1. Time evolution in the world-line representation for $2+1$ dimensions. The configuration returns either to itself without exchanging particles and has a positive weight or particles exchange, resulting in a negative sign. The topological nature becomes apparent when connecting the two world lines by sheet, which closes either to a cylinder or a Möbius strip.

an infinitesimal notation but understand that it refers to both discrete time formulations with finite time steps $\delta\tau$ and the infinitesimal limit.[2] Using a Hubbard-Stratonovich decomposition one rewrites the contribution of each of the interaction terms to the weight $\exp(-d\tau H)$ of one time step as

$$e^{-d\tau U c_{i\uparrow}^\dagger c_{i\uparrow} c_{i\downarrow}^\dagger c_{i\downarrow}} \to \int_{-\infty}^{\infty} d\rho_i e^{-\frac{\rho_i^2}{2d\tau|U|}+\rho_i(c_{i\uparrow}^\dagger c_{i\uparrow}+c_{i\downarrow}^\dagger c_{i\downarrow})}, \quad (2)$$

where ρ_i is one component of the auxiliary field. Here a particle-hole transformation is performed on one spin species in the case of repulsive interactions. Other choices of auxiliary field decouplings exist but do not improve the sign problem [5,21]. A discrete version, more common in practice [40], is discussed in Appendix B. Our derivation and its conclusions can be repeated for any such transformation with real fields.[3]

After the Hubbard-Stratonovich decomposition we obtain an action that is quadratic in the fermion field operators. One integrates out the fermion degrees of freedom, obtaining a partition function $Z = \int \mathcal{D}[\boldsymbol{\rho}(\tau)] Z_\uparrow[\boldsymbol{\rho}] Z_\downarrow[\boldsymbol{\rho}]$ that is a path integral over just the auxiliary field configurations. The weight of a specific configuration $\boldsymbol{\rho}(\tau)$ is given by

$$Z_\sigma[\boldsymbol{\rho}] = \det\left[1 + e^{\beta\mu_\sigma}\mathcal{T}\exp\int_0^\beta d\tau\, H^{\text{aux}}[\boldsymbol{\rho}(\tau)]\right], \quad (3)$$

where $\mathcal{T}$ indicates time ordering and the chemical potentials μ_σ may have been changed by the particle-hole transformation. The matrix H^{aux} is defined through the auxiliary field Hamiltonian:

$$\hat{H}^{\text{aux}}[\boldsymbol{\rho}(\tau)] = -t\sum_{\langle ij\rangle,\sigma} c_{i\sigma}^\dagger c_{j\sigma} + \sum_i \rho_i(\tau)\hat{n}_i$$
$$= \sum_{ij,\sigma} H_{ij}^{\text{aux}}(\tau) c_{i\sigma}^\dagger c_{j\sigma}. \quad (4)$$

In certain symmetric cases, for example in the spin-balanced attractive Hubbard model or the half-filled repulsive one, $Z_\uparrow$ and $Z_\downarrow$ have the same sign for each configuration, thus making all weights positive.

As for most QMC algorithms, the zero-temperature limit can be obtained by letting $\beta \to \infty$. In this way the evolution operator approaches the projector onto the ground state. Taking the expectation value of this operator on a trial wave function nonorthogonal to the ground state, one obtains the so-called projection-QMC scheme, for which all of our derivations can be repeated identically.

The origin of the sign problem in determinantal QMC methods has been controversial from the beginning. Already the first paper suggested that the sign problem should be absent for smooth auxiliary fields [4]. However, attempts to remove the sign problem by introducing a smoothing term to the action failed [36]. It has also been suggested that in a ground state projector version of the algorithm a topological sign problem may exist due to particle exchange similar to WL-QMC [22]. A similar claim was made based on an example in the adiabatic limit at $T = 0$, where a topologically nontrivial soliton was found to be responsible for the negative sign in a specific configuration [38]. The absence of a sign problem for smooth paths reappeared in recent claims based on a bosonization approach [27,28]. Following a different line of argument, it was suggested that the sign problem was merely an artifact of numerical instabilities and could be ignored [25,39]. However, these claims were refuted by comparing to numerically exact solutions on small clusters [26].

To investigate the role of time discretization and numerical inaccuracies in the sign problem, we performed simulations using $\delta\tau$ as small as $t/200$ and implemented a resilient numerical stabilization procedure and a 4096-bit precision version of the algorithm. We found that smaller time steps, numerical stabilization, and high precision improved the sign problem, but there remained configurations with negative sign even after smoothing the paths (i.e., cutting the high frequency components). This indicates an intrinsic sign problem even for smooth paths in the continuous time limit.

To elucidate the origin of these negative signs we discuss the structure of single-fermion modes in H_{aux}. While instantaneous eigenvectors $|\psi_n(\tau)\rangle$, defined by

$$H_{\text{aux}}(\tau)|\psi_n(\tau)\rangle = \varepsilon_n(\tau)|\psi_n(\tau)\rangle, \quad (5)$$

seem intuitive, the important ones are the *time integrated* eigenvalues and eigenstates of the evolution matrix $G(0;\beta) = \mathcal{T}\exp\int_0^\beta d\tau' H^{\text{aux}}[\rho(\tau')]$:

$$G(0;\beta)|\phi_n(0)\rangle = \lambda_n|\phi_n(0)\rangle. \quad (6)$$

We stress that this definition does not depend on smoothness or any periodicity of the evolution, and it is completely valid for the case of interaction expansion algorithms and zero-temperature methods (see Appendix C).

[2]As always in the definition of path integrals the integrand is well defined only at finite time steps $\delta\tau$. Using the notation of infinitesimals implies that the limit $\delta\tau \to 0$ is taken after performing all evaluations at finite $\delta\tau$

[3]We note the generic transformation $e^{-d\tau U c_\uparrow^\dagger c_\uparrow c_\downarrow^\dagger c_\downarrow} \to \int_{-\infty}^{\infty} d\rho P(\rho) e^{-\frac{\rho^2}{2d\tau|U|}+\rho(c_\uparrow^\dagger c_\uparrow + c_\downarrow^\dagger c_\downarrow)}$ with an arbitrary probability distribution P. Similar transformations can take into account particle-hole superpositions using a Bogoliubov transformation.

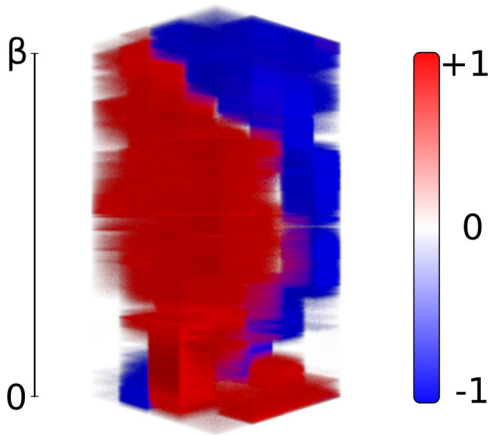

FIG. 2. Imaginary time evolution of the highest occupied state $|\phi_n(\tau)\rangle$ for a smoothed negative-sign configuration on a 4×4 Hubbard plaquette. Red (blue) color indicates regions of positive (negative) wave function.

We examined the evolved eigenvectors (which are the also the eigenstates of the time shifted evolution[4])

$$|\phi_n(\tau)\rangle = \mathcal{T}\exp\int_0^\tau d\tau' H^{\rm aux}[\rho(\tau')]|\phi_n(0)\rangle \tag{7}$$

for negative sign configurations and we found that there are always some that change sign during time evolution, i.e., $\lambda_n<0$. The evolution of one of these states is plotted in Fig. 2, where the negative and positive domain wind around each other, giving a negative weight.

Expressing the weight of Eq. (3) in terms of the λ_n, we obtain

$$Z_\sigma[\boldsymbol{\rho}] = \prod_n (1+\lambda_n e^{\beta\mu_\sigma}), \tag{8}$$

which is negative whenever an odd number of negative-sign single-particle states are more than 50% occupied, i.e., $|\lambda_n|>e^{-\beta\mu}$.

We now present a simple, smooth auxiliary field configuration that allows us to understand how the negative signs emerge. This configuration is given by the auxiliary field Hamiltonian

$$H^{\rm aux}(\tau)=\begin{pmatrix} v\sin(\tau) & -t & -t \\ -t & v\sin(\tau+2\pi/3) & -t \\ -t & -t & v\sin(\tau+4\pi/3)\end{pmatrix}, \tag{9}$$

which couples a periodic three-site chain to a rotating external field of strength v. Similar configurations can be constructed for longer chains. The noninteracting limit $v=0$ trivially has positive weights $\lambda_n=e^{-\beta\epsilon_n}$. Since $G(\tau;\beta)$ is real and has positive determinant, no eigenvalue can vanish, complex eigenvalues λ_n must come in complex conjugate pairs, and

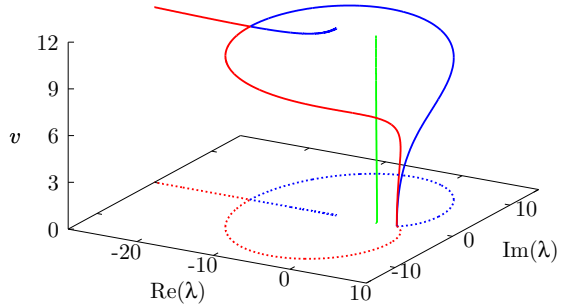

FIG. 3. Eigenvalues of the single-particle propagator $G(0;\beta)$ with $\beta=1$ as a function of field strength v of the auxiliary Hamiltonian (9). The dotted lines represent the projections of the paths onto the plane.

there must always be an even number of negative eigenvalues, as was sketched in Ref. [16].

By plotting, in Fig. 3, the eigenvalues of $G(0;\beta)$, we see that by increasing v a doubly degenerate positive real eigenvalue splits into a complex conjugate pair that winds around the $\lambda=0$ line and rejoins on the negative real axis. A sign problem can appear upon further increasing v beyond this critical value $v^*\approx 11.2$, as the pair splits into two different real negative eigenvalues, and one of the corresponding states becomes occupied and the other unoccupied. Increasing β shows $v^*\to 0$ such that in the zero-temperature limit the sign problem can occur for any interaction strength and only depends on the geometry of the auxiliary field configuration. This winding of pairs of eigenvalues around zero, to become negative, causes the bosonization treatment of Ref. [27] to break down (see Appendix D).

We turn now to the most general case, without assumptions on the size or nature of the system. The only requirement is that the weight of a configuration can be written as

$$w(c) = \det[1+G(0;\beta)]. \tag{10}$$

The sign of a single-particle state in the general case is understood as a geometric phase by decomposing the eigenvalues in Eq. (6) as $\lambda_n=e^{i\theta_n}\omega_n$ where $\omega_n>0$. The phases θ_n, given by

$$e^{i\theta_n} = \prod_{\tau=0}^{\beta}\langle\phi_n(\tau+d\tau)|\phi_n(\tau)\rangle, \tag{11}$$

are imaginary time versions of the Aharonov-Anandan (AA) phase, which is used to describe the geometric properties of nonadiabatic unitary evolution [29]. The *global* geometric phase θ determining the sign of the configuration is then obtained as the sum of the individual AA phases θ_n of the occupied levels, which in turn depend only on the geometric properties of the auxiliary field. The weights ω_n either diverge or vanish in the $\beta\to\infty$ limit, which means that a level is either fully occupied or completely empty, as expected in the case of zero thermal fluctuations.

As we see, θ can be nonzero even for smooth field configurations, a fact that was missed by Refs. [4,27]. Since the auxiliary Hamiltonian is real, and complex eigenvalues of $G(0;\beta)$ are always degenerate and thus do not contribute to the overall phase of the configuration, we only consider real

[4]One can verify it by directly applying the shifted evolution $G(\tau;\beta)=\mathcal{T}\exp\int_\tau^{\tau+\beta}d\tau' H^{\rm aux}[\rho(\tau')]$, where the auxiliary field is extended periodically. For projection methods the same applies by inserting the projection on the trial wave function at time β.

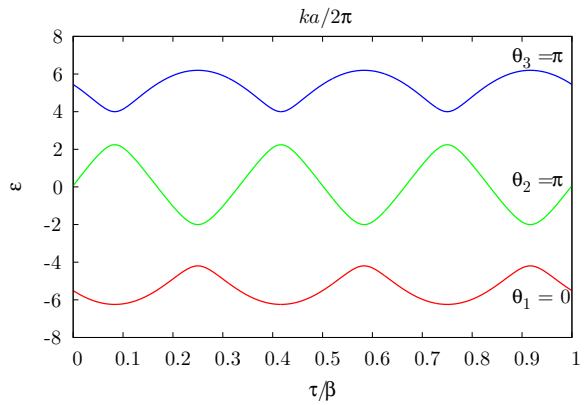

FIG. 4. Instantaneous levels of the Hamiltonian (9) for $v = 6$.

λ_n. For these eigenvalues, the wave functions $|\phi_n(\tau)\rangle$ can be chosen to be real at all times, implying that the AA phases θ_n are quantized to be either 0 or π. The phases vanish if the wave function can be chosen real and single-valued, i.e., $\psi(0) = \psi(\beta)$ at all times τ. However, it may not be possible to make such a choice globally continuous over $\tau \in [0,\beta]$, and the wave function may change sign during evolution, resulting in $\theta_n = \pi$.

When the evolution becomes *adiabatic*, such as if we stretch a smooth finite temperature configuration by taking $\beta \to \infty$, the Hamiltonian is locally constant and $e^{-\delta\tau H(\tau)}$ projects onto the instantaneous eigenvectors so that $|\psi_n(\tau)\rangle = |\phi_n(\tau)\rangle$. The weights then are $w_n = \exp[-\int_0^\beta \varepsilon_n(\tau)d\tau]$ and the AA phases θ_n reduce to Berry phases.

Our result relates the fermionic sign problem to the field of geometric phases arising from cyclic evolution [41–43]. Quantizations of these phases are known to appear as a consequence of symmetry and correspond to *topological invariants*, as, e.g., in the integer quantum Hall effect [44]. Recently these concepts are widely utilized in the field of symmetry protected topological (SPT) phases and topological insulators [45,46]. Extensive classification of topological insulators exists [47,48], assigning topological invariants to gapped single-particle Hamiltonians depending on their symmetries. Connecting systems with different topological invariants is guaranteed to give raise to metallic interface or edge states that are topologically protected against disorder.

The analogy between the our framework and topological materials can made more concrete by identifying the single-particle states of our model at a definite imaginary time τ with bands of a one-dimensional crystal, and relating τ to the crystal momentum k. Each band has a quantized AA $\theta_n = 0,\pi$ phase accumulated, moving across the Brillouin zone as illustrated in Fig. 4, that is a topological invariant and can only change by introducing complex gauge fields or closing the band gap. For nonadiabatic evolution, integrated eigenstates contain different contributions from the instantaneous ones. The sign of a configuration depends on which contributions are dominant, as we illustrate in Appendix E. This allows us to understand two core principles that allow sign-problem-free simulations.

First, in the presence of time-reversal-like symmetries, single-particle states come in Kramers pairs, with both states having the same geometric phase. As a consequence, the total phase winding vanishes, making the model sign-free, as shown in Refs. [16,18,19]. Second, the common wisdom that half-filled bipartite lattices are sign-problem free is shown to be a consequence of a topological constraint causing the negative eigenvalue pairs to be in even numbers (see Appendix F).

Our approach applies also to diffusion QMC (DMC) schemes, in which many-body states are generated by interpreting the elements of the Hamiltonian or evolution matrix as the transition matrix of a Markov process. DMC is conceptually similar to a zero-temperature version of WL-QMC and, as in the latter, sign problems can occur due to particle exchange. This led to the development of a family of DMC schemes that restrict the sampling to antisymmetric wave functions, in the hope of solving the sign problem [23,24]. However, even when formulating DMC explicitly in the space of Slater determinants there is still a residual sign problem that does not originate from particle exchange and bosonic collapse.

The topological origin of the sign problem discussed here corresponds to the residual one encountered in DMC and WL-QMC. In fact, a configuration in determinantal QMC can be mapped into a sum of configurations in DMC [49,50] and WL-QMC [51] by taking into account all possible permutations of the particles. Thus, DMC and WL-QMC are subject to two sign problems: one trivially due to Slater determinants being antisymmetric sums of configurations, and the residual topological one discussed in this paper.

Once the wave-function antisymmetry is taken into account, the exponential sign problem of fermionic QMC is due to a nontrivial topological invariant. Hence, negative signs cannot be simply removed by any local modification or basis change. Understanding the sign of Monte Carlo configurations in terms of Aharonov-Anandan phases of the single-particle eigenstates, and the connection to topological insulators and superconductors, clarifies long-standing open questions about the fermion sign problem [4,22,27,28,37], opening interesting perspectives for further studies, and providing a path towards the construction of a wider class of sign-problem-free models.

ACKNOWLEDGMENTS

We acknowledge discussions with K. Efetov, J. Gukelberger, E. Gull, J. Imriška, H.G. Matuttis, A.J. Millis, A. Muramatsu, O. Parcollet, C. Pépin, R. Scalettar, and P. Staar. This work was supported by the ERC Advanced Grant SIMCOFE, Microsoft Research, and the Swiss National Science Foundation through the National Competence Centers in Research NCCR QSIT and MARVEL. M.T. acknowledges hospitality of the Aspen Center for Physics, supported by NSF Grant No. 1066293.

APPENDIX A: THE NEGATIVE SIGN PROBLEM

The foundation of quantum Monte Carlo (QMC) simulation is a mapping of a quantum system to an equivalent classical one by expressing both the partition function

$$Z = \mathrm{Tr}\exp(-\beta H) = \sum_{c\in\Omega} w_c \tag{A1}$$

and the thermal expectation values of any observable,

$$\langle O\rangle = \frac{1}{Z}\mathrm{Tr}[O\exp(-\beta H)] = \frac{1}{Z}\sum_{c\in\Omega} O_c w_c, \tag{A2}$$

as a sum over set of "classical" configurations Ω. In the case of a path-integral representation this is the set of all path configurations, c is a specific path, w_c its weight, and O_c the contribution of the path to the expectation value of the observable O.

For non-negative weights $w_c \geqslant 0$, this classical system can be sampled by choosing a set of M configurations $\{c_i\}$ from Ω according to the distribution w_{c_i}. The average can then estimated by the sample mean

$$\langle O\rangle \approx \overline{O} = \frac{1}{M}\sum_{i=1}^{M} O_{c_i}, \tag{A3}$$

within a statistical error

$$\Delta O = \sqrt{\frac{\mathrm{Var}\, O}{M}(2\tau_O + 1)}, \tag{A4}$$

where $\mathrm{Var}\, O$ is the variance of O and τ_O is the integrated autocorrelation time of the sequence $\{O_{c_i}\}$.

The standard way of dealing with the negative weights w_c is to sample with respect to the absolute values of the weights $|w_c|$ and to assign the sign $s_c \equiv \mathrm{sgn}\, w_c$ to the quantity being sampled:

$$\begin{aligned}\langle O\rangle &= \frac{\sum_c O_c w_c}{\sum_c w_c}\\ &= \frac{\sum_c O_c s_c |w_c| \big/ \sum_c |w_c|}{\sum_c s_c |w_c| \big/ \sum_c |w_c|} \equiv \frac{\langle Os\rangle'}{\langle s\rangle'}.\end{aligned} \tag{A5}$$

While this allows Monte Carlo simulations to be performed, the errors increase exponentially with the particle number N and the inverse temperature β. To see this, consider the mean value of the sign $\langle s\rangle = Z/Z'$, which is just the ratio of the partition functions of the fermionic system $Z = \sum_c w_c$ with weights w_c and the bosonic system used for sampling with $Z' = \sum_c |w_c|$. As the partition functions are exponentials of the corresponding free energies, this ratio is an exponential of the differences Δf in the free energy densities [12,52,53]:

$$\langle s\rangle = \frac{Z}{Z'} = \exp(-\beta V \Delta f), \tag{A6}$$

where V is the volume of the system. As a consequence, the relative error $\Delta s/\langle s\rangle$ increases exponentially with particle number and inverse temperature:

$$\frac{\Delta s}{\langle s\rangle} = \frac{\sqrt{(\langle s^2\rangle - \langle s\rangle^2)/M}}{\langle s\rangle} = \frac{\sqrt{1-\langle s\rangle^2}}{\sqrt{M}\langle s\rangle} \sim \frac{e^{\beta V \Delta f}}{\sqrt{M}}. \tag{A7}$$

Similarly the error for the numerator in Eq. (7) increases exponentially, and the time needed to achieve a given relative error scales exponentially in V and β.

APPENDIX B: BSS ALGORITHM

For the discussions in the main paper we focus on the Blankenbecler-Scalapino-Sugar (BSS) algorithm [4], but note that our results apply more broadly to any auxiliary field algorithm. To explain this algorithm in more detail we split the Hubbard Hamiltonian into noninteracting and interacting parts:

$$H_0 = -t\sum_{\langle ij\rangle,\sigma} c^\dagger_{i\sigma} c_{j\sigma} - \sum_{i\sigma} \mu_\sigma c^\dagger_{i\sigma} c_{i\sigma}, \tag{B1}$$

$$H_I = U\sum_{i\sigma} c^\dagger_{i\uparrow} c_{i\uparrow} c^\dagger_{i\downarrow} c_{i\downarrow}. \tag{B2}$$

We then decompose the thermal density matrix using a Trotter decomposition

$$e^{-\beta H} = \lim_{N\to\infty} (e^{-\frac{\beta}{N}H_0} e^{-\frac{\beta}{N}H_I})^N \tag{B3}$$

coupled with either a continuous Hubbard-Stratonovich transformation

$$e^{-d\tau U c^\dagger_{i\uparrow} c_{i\uparrow} c^\dagger_{i\downarrow} c_{i\downarrow}} = \int_{-\infty}^{\infty} d\rho_i\, e^{\frac{\rho^2}{2d\tau U} + \rho_i (c^\dagger_{i\uparrow} c_{i\uparrow} - c^\dagger_{i\downarrow} c_{i\downarrow})}, \tag{B4}$$

where the auxiliary field ρ_i can take any real value, or alternatively a discrete one

$$\begin{aligned} e^{-d\tau U c^\dagger_{i\uparrow} c_{i\uparrow} c^\dagger_{i\downarrow} c_{i\downarrow}} &= 1 + \gamma c^\dagger_{i\uparrow} c_{i\uparrow} c^\dagger_{i\downarrow} c_{i\downarrow}\\ &= \frac{1}{2}\sum_{\sigma_i} (1 + \sqrt{\gamma}\sigma_i c^\dagger_{i\uparrow} c_{i\uparrow})(1 - \sqrt{\gamma}\sigma_i c^\dagger_{i\downarrow} c_{i\downarrow})\\ &= \frac{1}{2}\sum_{\rho_i} e^{-d\tau\rho_i (c^\dagger_{i\uparrow} c_{i\uparrow} - c^\dagger_{i\downarrow} c_{i\downarrow})}, \end{aligned} \tag{B5}$$

where $\gamma = 1 - e^{-d\tau U}$ and the auxiliary field ρ_i can have the two values $-\ln(1 \pm \sqrt{e^{d\tau U} - 1})/d\tau$. ρ_i diverges with $d\tau \to 0$, showing its fractal nature.

The partition function can be then rewritten as a sum over all configurations of the auxiliary field:

$$Z = \sum_{\{\rho_i(\tau)\}} \mathrm{tr}\left[\prod_{\tau=1}^{N} e^{-\frac{\beta}{N}H_0} e^{-d\tau\rho_i (c^\dagger_{i\uparrow} c_{i\uparrow} - c^\dagger_{i\downarrow} c_{i\downarrow})}\right] \tag{B6}$$

Since the product in the trace is composed of one-particle operators only (exponents are quadratic in the fermionic fields), the result can be obtained through the determinant of matrices in the single-particle picture:

$$Z = \sum_{\{\rho_i(\tau)\}} \det\left\{1 + \prod_{\tau=1}^{N} e^{-\frac{\beta}{N}H_0} e^{-d\tau\rho_i (c^\dagger_{i\uparrow} c_{i\uparrow} - c^\dagger_{i\downarrow} c_{i\downarrow})}\right\}, \tag{B7}$$

where the operators have been replaced by matrices. This can be written compactly using a time-ordered exponential

$$Z = \int \mathcal{D}[\rho(\tau)] \det\left\{1 + \mathcal{T}\exp\int_0^\beta d\tau\, H_{\mathrm{aux}}[\rho(\tau)]\right\}, \tag{B8}$$

having defined

$$H_{\mathrm{aux}}[\rho(\tau)] = H_{\mathrm{kinetic}} + \sum_i \rho_i(\tau)(\hat{n}_{i,\uparrow} - \hat{n}_{i,\downarrow}). \tag{B9}$$

Moreover, it can be decomposed into the product of determinants for the up and down spin components:

$$Z = \int \mathcal{D}[\rho(\tau)] Z_\uparrow[\rho] Z_\downarrow[\rho]. \tag{B10}$$

When the two contributions are equal, the algorithm is sign-problem free.

In the case of an attractive potential $U < 0$, one can obtain a decomposition of the interacting Hamiltonian with a field that couples to the total number of particles rather than the magnetization:

$$e^{-d\tau c_{i\uparrow}^\dagger c_{i\uparrow} c_{i\downarrow}^\dagger c_{i\downarrow}} = \sum_{\rho_i} e^{-d\tau \rho_i (c_{i\uparrow}^\dagger c_{i\uparrow} + c_{i\downarrow}^\dagger c_{i\downarrow})}. \tag{B11}$$

In this case, and in absence of any magnetic field making the up and down populations imbalanced, we have $Z_\uparrow = Z_\downarrow$ and the sign problem vanishes. The same is true when one looks at the half-filled repulsive case, which is related to the above by a particle-hole transformation.

The zero-temperature algorithm is obtained from the fact that in the long imaginary time limit the density matrix $\exp(-\beta H)$ becomes identical to the projector onto the ground state $|\psi_0\rangle$. Then one can start from a trial wave function $|\phi_T\rangle$ having finite overlap with the ground state. The decomposition above can then be applied to the following expressions:

$$\begin{aligned}
&\langle \phi_T | e^{-\beta H} | \phi_T \rangle \\
&\quad = \langle \phi_T | \int \mathcal{D}[\rho(\tau)] \mathcal{T} \exp \int_0^\beta d\tau \; H_{\text{aux}}[\rho(\tau)] | \phi_T \rangle, \qquad \text{(B12)} \\
&\langle \phi_T | e^{-\frac{\beta H}{2}} O e^{-\frac{\beta H}{2}} | \phi_T \rangle \\
&\quad = \langle \phi_T | \int \mathcal{D}[\rho(\tau)] \mathcal{T} \exp \int_{\beta/2}^\beta d\tau \; H_{\text{aux}}[\rho(\tau)] O \mathcal{T} \exp \\
&\qquad \times \int_0^{\beta/2} d\tau H_{\text{aux}} | \phi_T \rangle. \qquad \text{(B13)}
\end{aligned}$$

If the trial wave function is a Slater determinant, the expressions above reduce to a simple determinant, as in the case of the finite temperature algorithm.

A conceptually simpler view comes from the fact that the trial wave function can be thought of as the ground state of a trial Hamiltonian H_T. In this case we can rewrite (B12) as

$$\langle \phi_T | e^{-\beta H} | \phi_T \rangle = \lim_{\theta \to \infty} \text{tr}[e^{-\theta H_T} e^{-\beta H_0}]. \tag{B14}$$

From this representation one can trivially see that all the derivations in the main text can apply unchanged to the zero-temperature algorithm.

1. Arbitrary precision algorithm

To examine the sign of a configuration we implemented the BSS algorithm using arbitrary precision floating point numbers. This required the implementation of a QR algorithm, used to compute the determinant in Eq. (3) of the main text, and a double QZ step, to find the eigenvalues of the product G. Both algorithms were implemented following Ref. [54]. The power method was used to calculate eigenvectors for Fig. 2 of the main text.

The QZ step is a decomposition followed by an exchange of Q and R. The step is performed twice to keep all terms real:

$$\begin{aligned}
A = QR \to A' = Q^{-1} A Q = RQ = Q' R' \\
\to A'' = Q'^{-1} A' Q' = R' Q'. \qquad \text{(B15)}
\end{aligned}$$

Since this high precision algorithm is too slow for actual simulations it was primarily used to periodically check for correctness of weights. The algorithm gave the same results in all our tests for 4096 and 2048 bits of precision, but lower precision calculations using 1048 or 512 sometimes gave different results, in agreement with observed condition numbers that were as high as 10^{300}.

2. Stabilization procedure

At the core of the BSS algorithm is the calculation of the matrix

$$G(\beta) = \mathcal{T} \exp \int_0^\beta d\tau' H^{\text{aux}}[\rho(\tau')] \tag{B16}$$

in Eq. (3) of the main text. Using a discrete time formulation with M time steps, one has to compute a product of matrices

$$G_i = e^{-\delta_\tau H(\tau_i)} \tag{B17}$$

with $\delta_\tau = \beta / M$. The configuration weight is then computed as

$$Z = \det \left(1 + \prod_{i=1}^M G_i \right). \tag{B18}$$

However, multiplying a string of matrices results, in general, in a very ill-conditioned matrix. As the ratio between the largest and lowest eigenvalue diverges, information about the lowest eigenvalues and eigenstates is lost when the ratio between smallest and largest eigenvalues become of the order of roundoff. Calculations of the determinant of $G(\beta)$ then become inaccurate.

Numerical stabilization of the product of matrices with an acceptable accuracy is made possible by periodically decomposing the intermediate result using a rank-revealing decomposition, such as a singular value decomposition (SVD) or pivoting QR. An SVD is performed on each partial product of a subset consisting of m of the matrices G_i, corresponding to an evolution of time $\tau = m\delta_\tau$. We start with

$$\prod_{i=1}^m G_i \to U_k D_1 V_1^T. \tag{B19}$$

The next set of m matrices is then multiplied by UD and decomposed again:

$$\left(\prod_{i=m+1}^{2m} G_i \right) U_1 D_1 \to U_2 D_2 V_2^T. \tag{B20}$$

The procedure is repeated until the full product has been performed:

$$\prod_{i=1}^M G_i = U_{M/m} D_{M/m} V_{M/m}^t \cdots V_1^T. \tag{B21}$$

The value of m (or equivalently τ) should be chosen so that the condition number of the partial products can be stored within machine precision.

We used the arbitrary precision algorithm to check the numerical accuracy of negative sign configurations encountered with different numbers of decompositions. Our results confirmed that, while negative signs can creep into the simulation due to numerical errors with a low number of

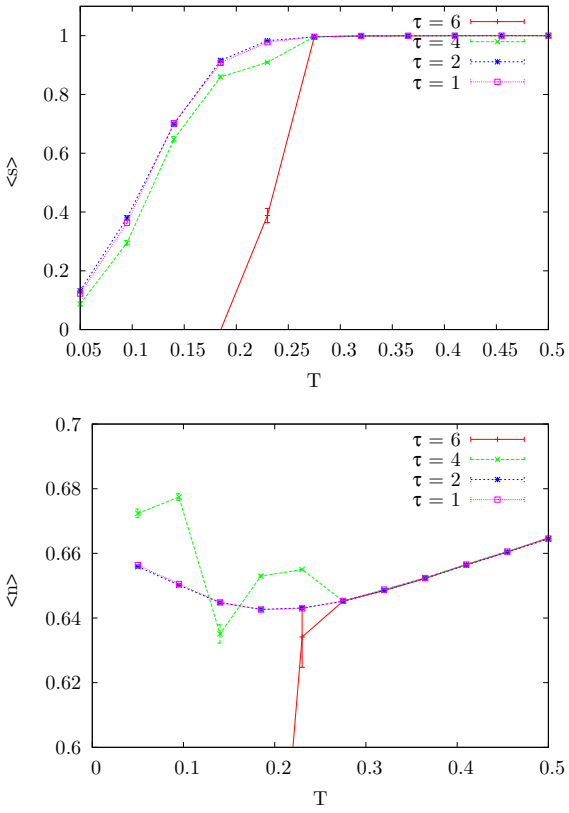

FIG. 5. Average sign s and number of particles n at $\mu = 0$ ($U/2$ below half-filling) as a function of temperature computed with varying distances τ between SVD decompositions on a 6×6 plaquette. With decreasing temperature, coarser decompositions start to develop a worse sign problem than finer grained ones. This influences even the simplest observables such as particle density.

decompositions, such errors disappear with a finer-grained stabilization scheme. This is corroborated by the results shown in Fig. 5.

Thus we confirm that there are no issues with numerical stability and precision issues provided that the stabilization scheme is performed correctly.

APPENDIX C: CONTINUOUS-TIME QMC

We can use the same derivations also to understand the sign problem in a CTQMC scheme. The following is based on the LCT-INT scheme detailed in Ref. [35]. Other schemes such as CT-INT and CT-AUX can be equally treated, since the weights are identical in both algorithms.

Continuous-time quantum Monte Carlo (CTQMC) methods stem from a perturbative expansion

$$Z = \operatorname{tr} e^{-\beta H} = \operatorname{tr}\left[e^{-\beta H_0} \mathcal{T} e^{-\int_0^\beta d\tau\, H_I(\tau)}\right] = \sum_{k=0}^{\infty} \frac{1}{k!} \operatorname{tr}\left[\mathcal{T} e^{-\beta H_0} \int_0^\beta d\tau_1 \cdots \int_0^\beta d\tau_k \prod_{i=1}^{k} (-H_I(\tau_i))\right], \tag{C1}$$

where (after a chemical potential shift)

$$H_I = -U \sum_x (1 - c^\dagger_{x\uparrow} c_{x\uparrow})(1 + c^\dagger_{x\downarrow} c_{x\downarrow}). \tag{C2}$$

The weight can be rewritten as

$$Z = \sum_k \int_0^\beta d\tau_1 \int_{\tau_1}^\beta \cdots \int_{\tau_{k-1}}^\beta d\tau_k \sum_{x_1,\ldots,x_k} w(c), \tag{C3}$$

where the factor $\frac{1}{k!}$ is taken care of by time ordering $\tau_1 < \tau_2 < \cdots < \tau_k$. $c = \{(x_1,\tau_1),\ldots,(x_k\tau_k)\}$ denotes a continuous-time path-integral configuration with k vertices. The weight can still be cast in the necessary form

$$w(c) = \det[1 + G(0;\beta)]. \tag{C4}$$

The analysis from the main text proceeds unchanged.

The matrix G is defined as

$$G(0;\beta) = e^{-(\beta-\tau_k)H_0} h(x_k) \cdots e^{-(\tau_2-\tau_1)H_0} h(x_1) e^{-\tau_1 H_0}, \tag{C5}$$

where

$$[\mathbf{h}(x_i)]_{x\sigma,y\sigma'} = U(\delta_{xy}\delta_{\sigma\sigma'} + \delta_{xx_i}\delta_{x_i y}\delta_{\sigma\uparrow}\delta_{\sigma'\uparrow} - \delta_{xx_i}\delta_{x_i y}\delta_{\sigma\downarrow}\delta_{\sigma'\downarrow}), \tag{C6}$$

CT-QMC now proceeds by sampling from all possible configurations c according to their weight $w(c)$. It can be more intuitive to imagine a smoothed vertex

$$\tilde{\mathbf{h}}(x_i) = \sqrt{\frac{2\pi}{\epsilon}} \int d\tau\, e^{\frac{-\tau^2}{2\epsilon^2}} e^{-\tau H_0} \mathbf{h}(x_i) e^{\tau H_0} \tag{C7}$$

and letting $\epsilon \to 0^+$.

While it is common to employ CTQMC in an auxiliary field framework, this is not necessary, as illustrated here and in Ref. [35]. This shows that the analysis in the present paper applies beyond auxiliary field schemes and adiabatic approximations.

APPENDIX D: RELATIONSHIP TO PRIOR WORK

In this section we discuss in more detail the relationship of our results to prior work, in particular the suggestion of a topological sign problem in projector QMC [22], Berry phases in spin models [37], and the suggestion that the sign problem can be removed by bosonization [27].

We were made aware of an unpublished result by J. Hirsch, where a negative-sign auxiliary field configuration was explicitly constructed to create two localized single-particle fermionic states, distant from each other, and then braid them [55]. In this configuration there is a clear link between the exchange of particles and the sign. This view, however, cannot be translated to the general case, where the single-particle states are delocalized.

1. Projection Monte Carlo

The first suggestion of a topological origin of the sign problem appears in the context of the projector quantum Monte Carlo (PQMC) method, attempting to explain the sign problem similar to the world line algorithm in terms of particle exchange [22].

In PQMC one takes the $T \to 0$ limits, which allows the trace over the thermal density matrix

$$\hat{G}(\rho,\beta) = \prod_{\tau=1}^{N} e^{-\frac{\beta}{N}H_0} e^{-d\tau\rho_i(c_{i\uparrow}^\dagger c_{i\uparrow} - c_{i\downarrow}^\dagger c_{i\downarrow})} \tag{D1}$$

for a particular auxiliary field configuration ρ to be replaced by a projection from a trial state $|\psi_T\rangle$ (as long as this state is not orthogonal to the ground state):

$$Z[\rho] = \langle\psi_T|\hat{G}(\beta)|\psi_T\rangle. \tag{D2}$$

By choosing a trial state that is a Slater determinant of p fermions described by the $p \times n$ matrix P,

$$|\psi_T\rangle = \prod_p (P_{p1}c_1^\dagger + \cdots + P_{pn}c_n^\dagger)|0\rangle, \tag{D3}$$

we can express the overlap of $|\psi_T\rangle$ with the time evolved state $\hat{G}(\beta)|\psi_T\rangle$ as a determinant in terms of the single-particle matrices:

$$\langle\psi_T|\hat{G}(\beta)|\psi_T\rangle = \det(P^T G(\beta) P) \tag{D4}$$

If, as is the case for the world-line Monte Carlo, the configuration comes back to itself, i.e., $|\psi_T\rangle \propto \hat{G}(\beta)|\psi_T\rangle$, it would be clear that each fermion has either come back to its original state or has exchanged with another particle. In this case the sign would be positive or negative depending on the sign of the permutation involved.

This simple picture is complicated in the current case since the time evolved state $\hat{G}(\beta)|\psi_T\rangle$ is, in general, not proportional to $|\psi_T\rangle$. Moreover, it cannot even be written as a Slater determinant of orthogonal vectors as the projection will squeeze the p single-particle wave functions that make up $|\psi_T\rangle$ towards the same ground state.

In Ref. [22] a Gram-Schmidt orthogonalization of the vectors is used to obtain the weight as the determinant of one orthogonal matrix Q times a positive-determinant matrix. The sign then depends on whether Q describes a *proper* or *improper* rotation (i.e., rotation plus reflection). Since the orthogonal matrix can be defined at each time step, after specifying a connection to uniquely identify Q at each step, one can see the evolution as an open curve in the space of orthogonal matrices.

The relationship between this representation of the many-body wave function and the Aharonov-Anandan phases of the single-particle states is an interesting topic and deserves additional study.

2. Spin Berry phase

An interpretation of the sign problem in terms of a spin Berry phase was suggested by Ref. [37]. There an auxiliary field decomposition of the Heisenberg Hamiltonian $H_I = J\sum_{\langle ij\rangle} \mathbf{s}_i \cdot \mathbf{s}_j$ is proposed. Decoupling the spins with an auxiliary vector field $\mathbf{\Delta}_i(\tau)$, the weight for a given field configuration is expressed as

$$Z = \int \mathcal{D}\mathbf{\Delta} Z[\mathbf{\Delta}] = \int \mathcal{D}\mathbf{\Delta} e^{-\int_0^\beta J^{-1}\sum_{\langle ij\rangle}\mathbf{\Delta}_i(\tau)\cdot\mathbf{\Delta}_j(\tau)d\tau} \times \mathrm{tr}\left[\mathcal{T}\exp\int_0^\beta d\tau \sum_i \mathbf{\Delta}_i(\tau)\cdot\mathbf{s}_i(\tau)\right]. \tag{D5}$$

The phases gained by the eigenvectors under imaginary time evolution are standard Berry phases of the decoupled spins and may generate a *phase problem* for the spin Hamiltonian. To our knowledge this paper is the first discussion of a Berry phase in a diffusive (imaginary time) context.

The paper then speculates that a similar Berry phase of spin fluctuations may be the origin of the fermion sign problem in the Hubbard model. However, this relationship is not worked out, and in particular because there is no clear relationship between the auxiliary vector field for the decomposition of spin models and the auxiliary scalar field used in fermionic models. Note also that the auxiliary field approach is not used for spin Hamiltonians, since it generally introduces a phase problem even in models that have no sign problem in a world-line formulation. As we have seen, while the origin of the sign problem is also a geometric phase in the Hubbard model, it is not related to the spin Berry phase of Ref. [37].

3. Bosonization

Efetov, Pépin, and Meier [27] suggested that bosonization can be used to remove the sign problem. In their approach the logarithm of the weight of a configuration is written as

$$\ln Z[\rho] = \int_0^1 \frac{\partial_v Z[v\rho]dv}{Z[v\rho]} + \ln Z[0] + 2\pi i n, \tag{D6}$$

where n is an arbitrary integer, as the phase of $\ln Z$ is only defined up to a multiple of 2π. This can be understood as obtaining the weight $Z[\rho]$ of a configuration starting from the free Hamiltonian $Z[0]$ and slowly ramping up the field strength. As long as the integral remains real, no sign change can occur in the weight. Whether this is true depends on the behavior of $1/Z[v\rho]$. Since the integrand is real, it might seem reasonable to assume that the integral is as well; this, however, assumes the absence of divergencies. Following the analysis in the main text, we now explicitly show how such divergencies arise. Making the dependence of the configuration weight on the strength of the auxiliary field v explicit, we obtain

$$Z[v\rho] = \prod_n [1 + e^{\beta\mu}\lambda_n(v)], \tag{D7}$$

for which the bosonization procedure gives

$$\ln Z[\rho] - \ln Z[0] = \sum_n \int_0^1 dv \frac{\lambda_n'(v)}{e^{-\beta\mu} + \lambda_n(v)} = \sum_n \int_{\gamma_n} d\lambda \frac{1}{e^{-\beta\mu} + \lambda}, \tag{D8}$$

where γ_n is the trajectory of the nth eigenvalue. We can see from our three-site example that one of the eigenvalues crosses the pole at $-e^{-\beta\mu}$ at some value of the field strength v. In this case the integrand must be rewritten using the regularization

$$\frac{1}{x} \to \mathcal{P}\frac{1}{x} \pm \pi i\delta(x), \tag{D9}$$

depending on whether it is regularized using the advanced or retarded Green function. Regardless of the choice, the integral will pick up a contribution πi for each eigenvalue crossing the pole, and the weight will be negative when the number of such crossings is odd. As we can see, divergencies are common

and linked to a change in the Berry phase of the states when increasing the field strength.

A different bosonization scheme was later suggested, which modifies the probability distribution to make all the weights positive [28]. While this method is expected to give different expectation values on finite size lattices, the authors argue that it will converge to the correct values the thermodynamic limit. However, this has not yet been demonstrated.

4. Solitonic solutions

A similar analysis to the present paper has been carried in Ref. [38]. The numerical precision obtainable with 32-bit and 64-bit floating point numbers was examined, concluding that several different methods to perform matrix computations (sparse matrix methods, Gaussian eliminations, and small rank updates) are essentially equivalent up to a certain condition number. It was then concluded that the results were correct when results in 32-bit and 64-bit precision agreed. Our findings confirm that this is the case by comparing finite and arbitrary calculations.

The authors also explicitly constructed an auxiliary-field configuration having a negative eigenvalue smaller than -1. This was achieved for the continuum limit in both space and time and in the ground state limit $\beta \to 0$. Since the constructed zero mode is a soliton and topologically nontrivial, the authors conclude that topological features of the auxiliary field and fermionic wave function may be the root cause for the sign problem. They identified two main problems in their conjecture related to the discretization of space and adiabaticity. First, solitonic solutions are qualitatively different in the continuum and on a lattice [38]. Second, their solution is an adiabatic one. As adiabatic configurations are a zero-probability set in the ground state limit, the topological origin remained a conjecture. Our proof of a topological invariant (the AA phase) being related to the sign even in the nonadiabatic limit confirms the conjecture of these authors.

Reference [38] also makes an important point that the fermionic weight $Z[\rho]$ can be written as a ratio of two bosonic weights:

$$\det[1 + G(0;\beta)] = \frac{\det[1 - G^2(0;\beta)]}{\det[1 - G(0;\beta)]}, \tag{D10}$$

where both the numerator and denominator of the righ-hand side can be written as a series with positive summands. However, the authors caution that when negative eigenvalues are present, this series becomes similar to

$$-1 = \tfrac{1}{1-2} = 1 + 2 + 2^2 + 2^3 + \cdots, \tag{D11}$$

i.e., a series that, while formally having a finite value, does not converge in practice when sampled via Monte Carlo. This shows once again that seemingly innocuous manipulations that appear to remove the sign problem may in fact also make the Monte Carlo estimates incorrect.

APPENDIX E: THE ADIABATIC LIMIT

Given a configuration ρ at temperature β, we can relate it to a second one ρ' at β' simply by scaling ("stretching")

$$\rho'(\tau) = \rho\left(\frac{\beta}{\beta'}\tau\right). \tag{E1}$$

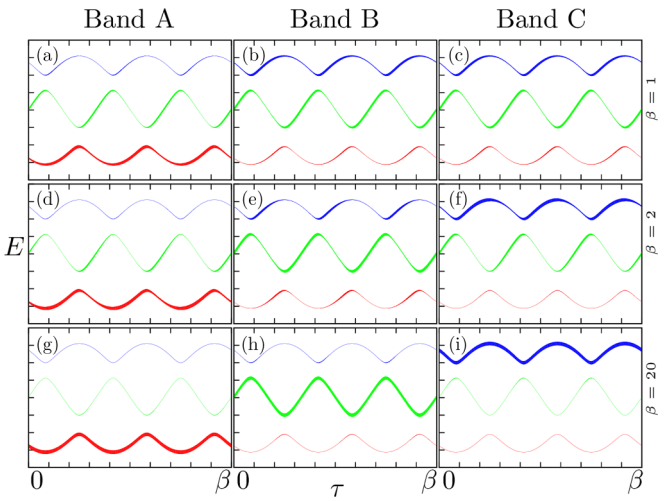

FIG. 6. The periodic eigenstates $|\phi(\tau)\rangle$ of the three band model are shown for different temperature β at $v = 6$. The line positions correspond to the instantaneous bands of Fig. 4 in the main text, and the line thickness is proportional to the overlap $|\langle\phi_n(\tau)|\psi_m(\tau)\rangle|^2$. At very low temperature (bottom row), the periodic eigenstates follow the instantaneous ones, as the configuration is stretched and the adiabatic approximation becomes valid. The lowest band A is always topologically trivial and does not give rise to a negative sign. At low temperatures the second and third bands B and C carry a π Berry phase and are topologically nontrivial. Since only band B is occupied, the overall configuration is negative. Raising the temperature (top row), the adiabatic approximation breaks down and bands B and C become degenerate and do not contribute a net phase to the weight.

In the limit $T \to 0$, the evolution can be taken piecewise constant, so that the element $e^{-\delta\tau H(\tau)}$ essentially projects onto the instantaneous eigenstates.

In Fig. 6 we illustrate the adiabatic limit for the smooth three-site configuration of the main text. We plot the overlap overlap $|\langle\phi_n(\tau)|\psi_m(\tau)\rangle|^2$ of the time-periodic eigenstates $|\phi_n(\tau)\rangle$ with the instantaneous ones $|\psi_m(\tau)\rangle$ at three temperatures: above the critical value for the appearance of a sign problem in this configuration, just below the critical value, and at very low temperature. One can observe how at high temperature two periodic eigenstates are degenerate and have the same overlaps. As the eigenvalues λ_n split at lower temperature, the overlaps also start to differ and the periodic states pick up a nontrivial phase from the instantaneous states. When the adiabatic approximation becomes valid (last row), each periodic state follows the corresponding band.

It is interesting to note that the phase in the intermediate temperature (middle row) is already nontrivial but the adiabatic approximation is not yet valid. This is evidenced by the fact that the periodic states do not follow the instantaneous ones, and the particles cross from one band to the other near the gaps.

APPENDIX F: BIPARTITE LATTICES

It is common wisdom that half-filled bipartite lattices can be simulated without a sign problem. However, until recently no rigorous proof has been devised and no general scheme for devising sign-problem-free simulations was known. We can show that this fact is the result of a topological obstruction,

that forces the number of occupied topologically nontrivial levels to be even.

In a half-filled, bipartite lattice with sublattices A,B, one can find a decomposition of $H[\rho]$ such that

$$e^{\tau H[\rho]}\eta = \eta e^{-\tau H[\rho]}, \tag{F1}$$

where $\eta = (-1)^x$ flips the wave-function sign sites belonging to sublattice B. Consequently we see that the full evolution matrix G satisfies

$$G^t\eta = \eta G^{-1}. \tag{F2}$$

Turning to the single-particle levels $G\psi_i = \lambda_i\psi_i$, we focus on the real nontrivial ones, i.e., $\lambda < 0$. While of course there is an even number of such eigenvalues, we need to prove that the number of those $\lambda_i < -1$ is even as well.

We first see, that due to the above chiral symmetry (F2),

$$\psi_i^{t*}\eta\psi_j = \psi_i^{t*}G^t\eta G\psi_j = \lambda_i\lambda_j\psi_i^{t*}\eta\psi_j, \tag{F3}$$

which implies that ψ_i is orthogonal (with respect to the metric η) to all other eigenvectors except ψ_j with $\lambda_j = \lambda_i^{-1}$. We call ψ_i eigenvectors corresponding to eigenvalue $\lambda_i < -1$ and $\tilde{\psi}_i$ those with eigenvalue λ_i^{-1}. Then we can choose

$$\psi_i^{t*}\eta\psi_j = 0, \tag{F4}$$

$$\tilde{\psi}_i^{t*}\eta\tilde{\psi}_j = 0, \tag{F5}$$

$$\psi_i^{t*}\eta\tilde{\psi}_j = \delta_{ij}, \tag{F6}$$

which means that we can identify $\tilde{\psi}_i(x) = (-1)^x\psi_i(x)$.

We now turn to show that a topological obstruction is present. If we take the restriction of G to one sublattice G_{AA} we see by continuity that it must have a positive determinant.[5]

In physical terms this means that if we start with a wave function restricted to the A sublattice, evolution will never make it vanish on the whole A sublattice, because the density difference between sublattices $\psi^t\eta\psi$ is conserved.

We now show how this leads to sign-problem-free simulations. The explicit form of G_{AA} is

$$\frac{1+\eta}{2}G\frac{1+\eta}{2} = \frac{1}{4}\sum_i \lambda_i(1+\eta)\psi_i\tilde{\psi}_i^{t*}\eta(1+\eta) + \lambda_i^{-1}(1+\eta)\tilde{\psi}_i\psi_i^{t*}\eta(1+\eta), \tag{F7}$$

but since (F4)–(F6) imply $\tilde{\psi}_i = \eta\psi_i$, we have

$$\frac{1+\eta}{2}G\frac{1+\eta}{2} = \frac{1}{4}\sum_i \left(\lambda_i+\lambda_i^{-1}\right)(1+\eta)\psi_i\psi_i^{t*}(1+\eta) \tag{F8}$$

and consequently

$$\det G_{AA} = \prod_i \left(\lambda_i + \lambda_i^{-1}\right) > 0, \tag{F9}$$

which proves that there are an even number of $(\lambda_i,\lambda_i^{-1})$ pairs and the determinant $\det(1+G)$ is positive.

An algebraic proof that takes care of the case with degenerate eigenvalues was found on the mathematical website MathOverflow [56] through the open collaboration of many researchers. Unlike the present proof, the full mathematical statement generalizes to degenerate eigenvalues. Since such configurations are a null measure set in any case, this is of marginal importance for actual simulations. The full theorem (nicely summarized in Terence Tao's blog [57]) also characterises completely the set of interactions that can be simulated without a sign problem and determines the invariants associated with negative-sign sectors.

[5] In fact, if the determinant vanishes, we would have a state $(v,0)$ such that $G_{AA}v = 0$,

$$v^\dagger v = (v^t,0)\eta\begin{pmatrix} v \\ 0\end{pmatrix} = (v^t,0)G^t\eta G\begin{pmatrix} v \\ 0\end{pmatrix} = -v^t G_{BA}^t G_{BA} v,$$

which is clearly contradictory, hence $\det G_{AA}$ cannot vanish and by extension cannot become negative.

[1] N. Metropolis and S. Ulam, J. Am. Stat. Assoc. **44**, 335 (1949).
[2] D. C. Handscomb, Math. Proc. Cambridge Philos. Soc. **60**, 115 (1964).
[3] M. Suzuki, Prog. Theor. Phys. **56**, 1454 (1976).
[4] R. Blankenbecler, D. J. Scalapino, and R. L. Sugar, Phys. Rev. D **24**, 2278 (1981).
[5] J. E. Hirsch and R. M. Fye, Phys. Rev. Lett. **56**, 2521 (1986).
[6] D. M. Ceperley and B. J. Alder, Phys. Rev. Lett. **45**, 566 (1980).
[7] W. M. C. Foulkes, L. Mitas, R. J. Needs, and G. Rajagopal, Rev. Mod. Phys. **73**, 33 (2001).
[8] G. G. Batrouni, V. Rousseau, R. T. Scalettar, M. Rigol, A. Muramatsu, P. J. H. Denteneer, and M. Troyer, Phys. Rev. Lett. **89**, 117203 (2002).
[9] G. E. Astrakharchik, J. Boronat, J. Casulleras, and S. Giorgini, Phys. Rev. Lett. **93**, 200404 (2004).
[10] K. Schmidt and S. Fantoni, Phys. Lett. B **446**, 99 (1999).
[11] R. Gupta, G. W. Kilcup, and S. R. Sharpe, Phys. Rev. D **38**, 1278 (1988).
[12] E. Y. Loh, J. E. Gubernatis, R. T. Scalettar, S. R. White, D. J. Scalapino, and R. L. Sugar, Phys. Rev. B **41**, 9301 (1990).
[13] M. Troyer and U.-J. Wiese, Phys. Rev. Lett. **94**, 170201 (2005).
[14] S. A. Cook, in *Proceedings of the Third Annual ACM Symposium on Theory of Computing*, STOC '71 (ACM, New York, NY, 1971), pp. 151–158.
[15] S. Chandrasekharan and U.-J. Wiese, Phys. Rev. Lett. **83**, 3116 (1999).
[16] C. Wu and S.-C. Zhang, Phys. Rev. B **71**, 155115 (2005).
[17] S. Chandrasekharan, Phys. Rev. D **82**, 025007 (2010).
[18] E. Berg, M. A. Metlitski, and S. Sachdev, Science **338**, 1606 (2012).
[19] E. F. Huffman and S. Chandrasekharan, Phys. Rev. B **89**, 111101 (2014).

[20] S. Sorella, S. Baroni, R. Car, and M. Parrinello, Europhys. Lett. **8**, 663 (1989).
[21] G. G. Batrouni and R. T. Scalettar, Phys. Rev. B **42**, 2282 (1990).
[22] A. Muramatsu, G. Zumbach, and X. Zotos, Int. J. Mod. Phys. C **03**, 185 (1992).
[23] S. Zhang and M. H. Kalos, Phys. Rev. Lett. **67**, 3074 (1991).
[24] M. H. Kalos and F. Pederiva, Phys. Rev. Lett. **85**, 3547 (2000).
[25] H.-G. Matuttis and N. Ito, Int. J. Mod. Phys. C **16**, 857 (2005).
[26] E. Y. Loh, J. E. Gubernatis, R. T. Scalettar, S. R. White, D. J. Scalapino, and R. L. Sugar, Int. J. Mod. Phys. C **16**, 1319 (2005).
[27] K. B. Efetov, C. Pépin, and H. Meier, Phys. Rev. Lett. **103**, 186403 (2009).
[28] K. B. Efetov, C. Pépin, and H. Meier, Phys. Rev. B **82**, 235120 (2010).
[29] Y. Aharonov and J. Anandan, Phys. Rev. Lett. **58**, 1593 (1987).
[30] J. B. Anderson, J. Chem. Phys. **65**, 4121 (1976).
[31] J. L. DuBois, E. W. Brown, and B. J. Alder, arXiv:1409.3262.
[32] A. N. Rubtsov, V. V. Savkin, and A. I. Lichtenstein, Phys. Rev. B **72**, 035122 (2005).
[33] E. Gull, P. Werner, O. Parcollet, and M. Troyer, Europhys. Lett. **82**, 57003 (2008).
[34] E. Gull, A. J. Millis, A. I. Lichtenstein, A. N. Rubtsov, M. Troyer, and P. Werner, Rev. Mod. Phys. **83**, 349 (2011).
[35] M. Iazzi and M. Troyer, Phys. Rev. B **91**, 241118 (2015).
[36] D. Scalapino (private communications).
[37] J. Samson, Int. J. Mod. Phys. B **07**, 593 (1993).
[38] J. Gubernatis and X. Zhang, Int. J. Mod. Phys. C **05**, 599 (1994).
[39] H.-G. Matuttis and N. Ito, J. Phys. Soc. Jpn. **70**, 1519 (2001).
[40] J. E. Hirsch, Phys. Rev. B **28**, 4059 (1983).
[41] M. V. Berry, in *Proceedings of the Royal Society of London A: Mathematical, Physical and Engineering Sciences*, Vol. 392 (The Royal Society, London, 1984), pp. 45–57.
[42] F. Wilczek and A. Shapere, *Geometric Phases in Physics*, Vol. 5 (World Scientific, Singapore, 1989).
[43] C. A. Mead, Rev. Mod. Phys. **64**, 51 (1992).
[44] D. J. Thouless, M. Kohmoto, M. P. Nightingale, and M. den Nijs, Phys. Rev. Lett. **49**, 405 (1982).
[45] M. Z. Hasan and C. L. Kane, Rev. Mod. Phys. **82**, 3045 (2010).
[46] X.-L. Qi and S.-C. Zhang, Rev. Mod. Phys. **83**, 1057 (2011).
[47] A. P. Schnyder, S. Ryu, A. Furusaki, and A. W. W. Ludwig, Phys. Rev. B **78**, 195125 (2008).
[48] A. Kitaev, AIP Conf. Proc. **1134**, 22 (2009).
[49] S. Fahy and D. R. Hamann, Phys. Rev. B **43**, 765 (1991).
[50] S. Zhang, J. Carlson, and J. E. Gubernatis, Phys. Rev. B **55**, 7464 (1997).
[51] J. E. Hirsch, Phys. Rev. B **34**, 3216 (1986).
[52] N. Hatano and M. Suzuki, Phys. Lett. A **163**, 246 (1992).
[53] D. M. Ceperley, in *Monte Carlo and Molecular Dynamics of Condensed Matter Systems* (Editrice Compositori, Bologna, 1996).
[54] W. H. Press, S. A. Teukolsky, W. T. Vetterling, and B. P. Flannery, *Numerical Recipes 3rd Edition: The Art of Scientific Computing*, 3rd ed. (Cambridge University Press, New York, 2007).
[55] R. T. Scalettar (private communications).
[56] http://mathoverflow.net/questions/204460/how-to-prove-this-determinant-is-positive (2015).
[57] T. Tao, https://terrytao.wordpress.com/2015/05/03/the-standard-branch-of-the-matrix-logarithm/ (2015).